湖南大学学报（自然科学版）
Journal of Hunan University (Natural Sciences)

第 50 卷 第 1 期
2023 年 1 月

Available online at http://jonuns.com/index.php/journal/index

Vol. 50 No. 1
January 2023

Open Access Article https://doi.org/10.55463/issn.1674-2974.50.1.20

Prediction and Investigation of the Interactive Impact of Shell Thickness and Infill Density on the Mechanical Properties, and the Mass of ABS Prints

Aqeel S. Bedan, Tahseen F. Abbas*, Emad A. Hussein

Department of Production Engineering and Metallurgy, University of Technology, Baghdad, Iraq

* Corresponding author: tahseen.f.abbas@uotechnology.edu.iq

Received: December 29, 2022 / Revised: January 15, 2023 / Accepted: January 25, 2023 / Published: February 28, 2023

Abstract: Shell thickness and infill density are key parameters for determining mechanical stability of a printed part when subjected to stress. This study aimed to establish models for predicting responses, specifically compressive strength, relative strength, and weight, and to analyze the interactive effects of both shell thickness and infill density on ABS prints, which were evaluated by conducting compression tests. For this purpose, the interactive effects of different shell thicknesses (0.4, 0.8, 1.2, 1.6, and 2.0 mm) and different infill densities (0%, 25%, 50%, 75%, and 100%) on the considered response variables, namely, compressive strength, relative strength, and material consumption of ABS prints were investigated. According to the results of the experiments, a specimen printed from ABS with a 75% infill density and a shell thickness of 2 mm has the highest relative compressive stress (1645 N/g). The evaluation of the effectiveness of the proposed prediction models was confirmed by comparing the measured data with the predicted data, which showed that the quadratic fit models presented in this study are suitable for all considered response variables. The model fits the data well, with a maximum error of 6.2%. By estimating the compressive strength, relative strength, and material consumption in relation to process parameters before manufacturing the FDM parts, the developed prediction models will assist practitioners in reducing the number of experimental works, resulting in material savings, reduced printing time, and reduced energy consumption.

Keywords: fused deposition modeling parameters, acrylonitrile butadiene styrene, mechanical properties, mass, prediction models.

预测和研究壳厚度和填充密度对机械性能和防抱死制动系统打印质量的交互影响

摘要：外壳厚度和填充密度是确定打印部件在承受压力时的机械稳定性的关键参数。本研究旨在建立预测响应的模型，特别是抗压强度、相对强度和重量，并分析壳厚度和填充密度对防抱死制动系统打印的交互影响，这些通过压缩测试进行评估。为此，不同壳厚度（0.4、0.8、1.2、1.6 和 2.0 毫米）和不同填充密度（0%、25%、50%、75%和 100%）对所考虑的响应变量的交互影响 ，即，研究了防抱死制动系统印刷品的抗压强度、相对强度和材料消耗。根据实验结果，由填充密度为 75%、壳厚度为 2 毫米的防抱死制动系统打印的试样具有最高的相对压应力(1645 氮/克)。通过将测量数据与预测数据进行比较，证实了所提出的预测

模型的有效性评估，这表明本研究中提出的二次拟合模型适用于所有考虑的响应变量。该模型与数据拟合良好，最大误差为 6.2%。通过在制造频分复用零件之前估算与工艺参数相关的抗压强度、相对强度和材料消耗，开发的预测模型将帮助从业者减少实验工作的数量，从而节省材料、减少打印时间和能源消耗 消耗。

关键词：熔融沉积建模参数、丙烯腈丁二烯苯乙烯、机械性能、质量、预测模型。

1. Introduction

The fundamental principles of product manufacturing are subtractive, formative, and additive manufacturing (AM). The most recently exploited of these three is additive manufacturing, which uses material deposition in layers to fabricate parts from a computer-aided design (CAD) model. The fundamental idea behind additive manufacturing is the creation of a digital model on a computer, which is later cut into 2D cross-sections and transferred to an AM machine to create the physical product layer by layer [1]. Three-dimensional (3D) printing, also known as additive manufacturing (AM), works by selectively joining materials from a 3D CAD (Computer-Aided Design) model of the desired part layer by layer [2]. The three construction categories of powder sintering or fusion, liquid solidification, and material deposition are the foundation for several additive manufacturing technologies [3]. These techniques include digital light projection (DLP), stereolithography apparatus (SLA), laminated object manufacturing (LOM), selective laser sintering (SLS), fused deposition modeling (FDM), and electron beam melting [4]. FDM is the most widely used of these 3D printing techniques due to its advantages over others, including ease of use, replacement ease, material choice, cost-effective maintenance, and use of non-hazardous build material. [5]-[6]. The main parts of the FDM printing machine are shown in Figure 1.

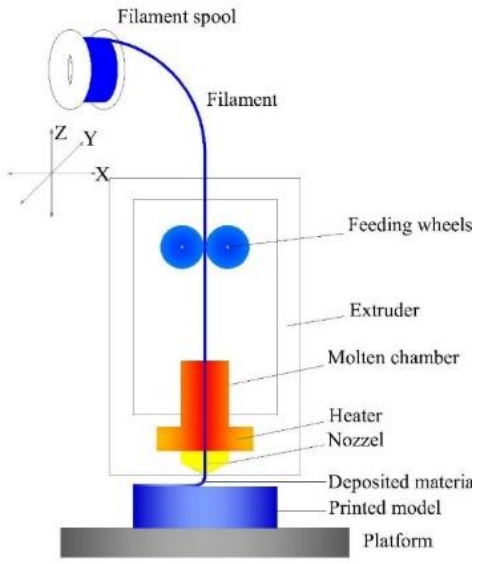

Fig. 1 Scheme of FDM machine (Developed by the authors)

The extruder moves along the x-y plane, allowing the printer to move in three directions (x, y, and z). FDM printers are computer-aided design (CAD) models that are printed into physical parts using programmed extrusion machines. The process involves converting CAD files to 3D STL file formats and dividing the CAD model into successive layers that are printed in succession. These layers are printed one by one using thermoplastic materials through a nozzle, which deposits the layers onto the printing platform [7].

The impact of the printing parameters on the mechanical characteristics of a 3D-printed object using FDM technology has been the subject of several studies. As reported in [8], the impact of cross-section geometry and layer thickness on the compression and tensile characteristics of 3D-printed ABS. The tensile strength, yield strength, and elastic modulus of manufactured components were tested as a function of design factors, including the infill density, nozzle diameter, layer thickness, and raster angle [9]. The effect of parameters was investigated in [10], including the type of infill pattern, infill density, shell thickness, and printing temperature, on the tensile strength of samples. There have been a few studies on acrylonitrile butadiene styrene (ABS), and most of these have only looked at the effect of process parameters on tensile or compressive strength.

The novelty of this study is the development of multiple regression models that predict the relationship between the response and the process factors, to improve the capabilities of the multifunctional FDM process by reducing the amount of material while increasing the relative strength of the prints, thus resulting in material savings, reduced printing time, and reduced energy consumption.

2. Materials

2.1. Materials in the FDM Process

Only a few raw materials were available when the FDM technique first emerged, the most popular of which were polylactic acid (PLA) and acrylonitrile butadiene styrene (ABS) [11]. This was one of the major obstacles this technology faced when it first came into existence. However, because of its high

technology capabilities and low cost, many researchers have been motivated to discover new raw materials, which has helped it gain widespread adoption and create new applications for technology that did not previously exist. There are numerous FDM filament suppliers in the market. Today, FDM printing employs a range of thermoplastic filaments including nylon, ABS, PLA, polycarbonate (PC), polyether-ether-ketone (PEEK), and other composites. However, the most common thermoplastics used in FDM 3D printers are still ABS and PLA [12]. ABS is an acrylonitrile butadiene styrene-based thermoplastic copolymer. The three structural units of the copolymer provide a balance of properties, with acrylonitrile supplying heat resistance, butadiene providing excellent impact strength, and styrene supplying rigidity. Because of its resistance to chemicals, heat, and physical effects, it is an excellent base material for a wide range of applications in various industries, including automobiles, medical appliances, electrical appliances, sports equipment, and construction applications [13]. ABS is chemically resistant to a wide range of solvents and acids. A closed printer must maintain heat during manufacturing to print ABS material correctly. This will prevent it from shrinking during printing and causing problems, such as warping or cracking [14].

2.2. Print Sections

In FDM printing, the print is performed sequentially in four different sections, as shown in Fig. 2. The first section of the 3D print is the shell, which are the walls of the print and are printed as a boundary parameter. They are divided into two sections, namely, the bottom and top layers. The bottom layer is the print layer, which is printed facing the printing build plate. This is the initial layer of the printing process. The top layer is the topmost or final layer of the print that is printed facing the nozzle. The infill, which is the fourth section, is contained between the shells, the bottom layer, and the top layer. Infill is the internal print structure that helps increase the mechanical stability of printed parts. Infill is performed in different patterns and is customizable according to the requirements [15]. Infill patterns are crucial for every print as they directly determine the strength of the part.

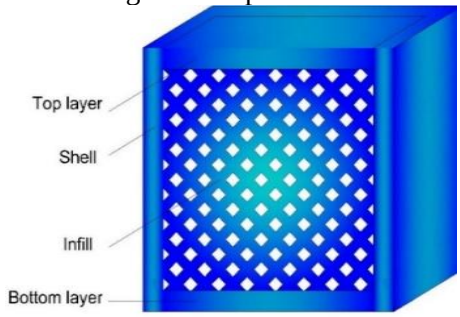

Fig. 2 Print sections (Developed by the authors)

2.3. Design of Experiments

Full and fractional factorial designs are the most commonly used experimental designs. A factorial design is a type of designed experiment that allows for investigating the effects of multiple factors on a response. When experimenting, varying the levels of all factors simultaneously rather than individually allows for capturing the interactions between the factors. A full factorial-designed experiment includes all possible level combinations for all factors. The total number of experiments required to investigate k factors at two levels is 2^k. The design of two factors, namely, shell thickness and infill density, was used in this work. Each factor was studied at five levels, i.e, a "5^2-factorial design" was applied.

3. Methods

3.1. Process Control Parameters

Two process control parameters, shell, and infill, that are likely to affect the mechanical properties and weight of FDM prints are adopted and studied extensively in this work.

3.2. Shell

Shells are the number of layers on the outside of a print. For FDM printing, shells are always the first areas to be printed per layer. Having a thick shell protects the infill well and provides good support for the structures. However, printing a thick shell has its drawbacks [16].

3.2.1. Shell Settings

Shell settings can be altered using slicing software, which is used to convert the CAD model into defined G-codes based on which the printer operation is started. The advantage of additional shell thickness is that the mechanical strength of the product will not be compromised, especially during post-manufacturing processing.

3.2.2. Shell Thickness

It is advisable to keep the shell thickness as a multiple of the nozzle diameter for easy configuration. Five different shell thicknesses, 0.4, 0.8, 1.2, 1.6, and 2.0 mm, were used in this work to examine their effects on the compressive strength, relative strength, and weight of the prints.

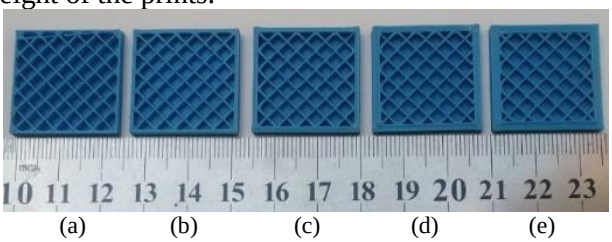

(a) (b) (c) (d) (e)

Fig. 3 Various shell thicknesses: (a) 0.4, (b) 0.8 mm, (c) 1.2 mm, (d) 1.6 mm, (e) 2 mm (Developed by the authors)

The diagram in Fig. 3 shows the appearance of various shell settings on a partially completed model.

3.3. Infill

Infill is the print material used to print support structures in the interior of the object to increase its mechanical strength. It directly corresponds to the density of the objects as it involves filling the voids in the shells of the objects. Infill is generally expressed in terms of volume density percentage [17]. The greater the infill percentage, the greater the mechanical stability and strength of the part, but the greater the time it takes to print.

3.3.1. Infill Settings

Similar to that shell settings, infill can also be modified using the slicing software used for the particular printer. The infill setting also has some prerequisites that need to be applied while configuring the numbers in the slicing software. The interior density of the model is indicated by the infill percentage. This setting spans from 0%, representing a hollow model, to 100%, pertaining to a fully solid one [18].

3.3.2. Infill Density

The amount of thermoplastic used in the printed structure depends on the infill density. With a higher fill density, the part is a little bit stronger because there is more thermoplastic material inside the prints. Instead of using a specific unit of measurement, the infill density is calculated as a percentage. It appears obvious that a completely solid model would be the strongest option. However, increasing the amount of infill, particularly for larger models with expansive internal spaces, can significantly impact both the cost and print time [19]. Maintaining a considerable level of infill percentage for a fully functioning mechanical part is essential since it requires strength to withstand a considerable amount of stress and strain.

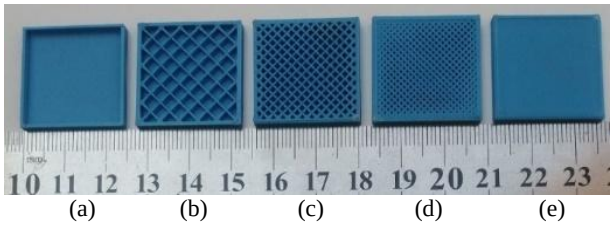

(a) (b) (c) (d) (e)

Fig. 4 Various percentages of infill density: (a) 0%, (b) 25%, (c) 50%, (d) 75%, (e) 100% (Developed by the authors)

Five levels of infill density of 0%, 25%, 50%, 75%, and 100% infill, as shown in the partially completed models in Fig. 4, were used in this work to examine their effects on the relative compressive strength and weight of the prints.

3.3.3. Infill Patterns

This is not fixed and can be altered. The popular infill patterns used in some of the 3D printers include rectangular, triangular, concentric, and the standard honeycomb pattern. The rectangular pattern is one of the simpler ones for printing using FDM printers, which focuses on applying equal strength throughout the shell, thus making the part durable. The rectangular pattern does not require any sort of additional infill bridging [20]. Due to its grid of parallel and perpendicular extrusions, rectangular infill is the only type that can produce a 100% dense part. For these reasons, the rectangular pattern illustrated in Fig. 5 was used in this work.

Fig. 5 A slice of a specimen with a rectangular infill (Developed by the authors)

3.4. Process Flow Steps

To slice a CAD model into horizontal layers and create the tool paths necessary for the extrusion head, the model must first be created in an STL file, with AutoCAD or another design program. The model then needs to be imported into slicing software. The following is a list of the building steps.

1. Use Cura's software to import the CAD model's STL file, which divides the model into horizontal layers.
2. Make the extrusion head's tool paths. The temperature-controlled FDM extrusion head receives the ABS material, which is heated to a semi-liquid state.
3. The head extrudes and deposits the material in 0.2 mm-thick layers in the X and Y coordinates, one layer at a time, onto a base.
4. When a layer is complete, the head advances in the Z direction to the subsequent layer.
5. Each layer is precisely extruded, and the layers are then bonded and solidified.
6. The printed object solidifies into a three-dimensional component.

3.5. Specimen Fabrication

An Ultimaker+2 printer was used to produce all the specimens. In this series of experiments, a 0.40 mm-diameter brass nozzle was used. It was demonstrated in [21] how the color of the filament affects the strength of its products when all other characteristics are the same. Thus, a filament of the same color (blue) in this work was used. All the experiments using the same values for the printing factors:

- Nozzle diameter (0.4 mm);
- Extruder temperature (235 °C);
- Heated bed temperature (105 °C);
- The thickness of the first and succeeding layers (0.2 mm);

- Printing speed for subsequent layers (30 mm/s).

The sample was positioned in the middle of the printer bed. Cura slicer software was used to create the G-code file. Fig. 6 illustrates the standard specimens used for the compression test, with the specimen geometry following the specifications outlined in ASTM D695.

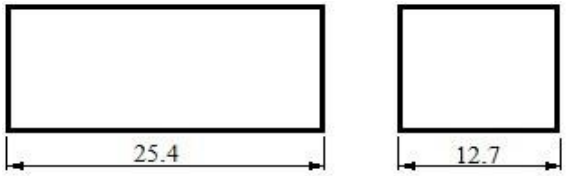

Fig. 6 Geometrical data of the specimen for the compression tests (Developed by the authors)

An ABS filament of diameter 1.75mm was used to print twenty-five (5^2) specimens for the compression tests, as shown in Fig. 7. The specimens were fabricated based on the load applied to the component.

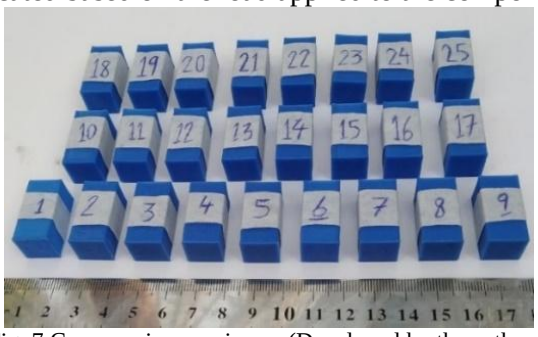

Fig. 7 Compression specimens (Developed by the authors)

A digital caliper was used to precisely measure the real external data for each printed specimen, and the measurements were read from an LCD, as shown in Fig. 8.

Fig. 8 Measuring the external dimensions of a compression specimen using a digital caliper (Developed by the authors)

The mass of each specimen was determined using digital analytical scales, as shown in Fig. 9 and the measurement results were rounded to two decimal places.

Fig. 9 Specimens weighed on a digital scale (Developed by the authors)

3.6. Mechanical Testing

Compression tests were carried out as per standard procedure until the part ruptured, at which point the load-strain relationship was established for each specimen. Specimen compression tests were performed on a standard universal electromechanical testing machine with a digital control system, and the specimens were fixed, as illustrated in Fig. 10.

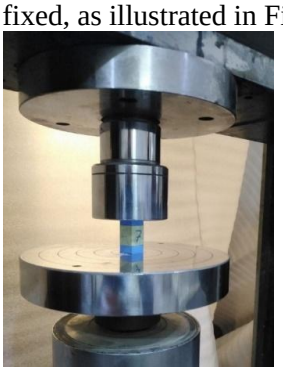

Fig. 10 Specimen compression test (Developed by the authors)

The tests were conducted at a constant speed of 5 mm/min until the specimen was destroyed. Displacements and loads were measured during the tests.

4. Results and Discussion

4.1. Results of the Compression Test

The collected mechanical data were obtained from the compression tests conducted on the 25 specimens with five families, which is summarized in Table 1. From these data, it is possible to obtain the relative compressive stress *RS* for each specimen by using Equation (1).

$$RS = \frac{F}{M} \quad (1)$$

where:
RS - relative strength [N/g];
F - fracture load [N];
M - the mass of the specimen [g].

Table 1 Collected mechanical data obtained from the compression tests conducted on the five families of specimens

Specimen (family)	Shell thickness [mm]	Infill density [%]	Specimen mass [g]	Comp. strength [MPa]	Fracture Load [kN]	Relative strength [N/g]
1(1)	0.4	0	0.86	1.562	0.252	293
2(1)	0.4	25	1.92	12.715	2.051	1068
3(1)	0.4	50	2.90	26.164	4.222	1455
4(1)	0.4	75	3.75	36.809	5.953	1587

Continuation of Table 1

5(1)	0.4	100	4.63	40.386	6.511	1406
6(2)	0.8	0	1.37	6.531	1.055	770
7(2)	0.8	25	2.27	18.198	2.919	1285
8(2)	0.8	50	3.06	27.632	4.455	1455
9(2)	0.8	75	3.94	38.042	6.141	1559
10(2)	0.8	100	4.63	41.187	6.643	1434
11(3)	1.2	0	1.87	13.293	2.144	1146
12(3)	1.2	25	2.55	21.598	3.482	1365
13(3)	1.2	50	3.32	31.053	5.007	1508
14(3)	1.2	75	4.05	39.847	6.427	1586
15(3)	1.2	100	4.63	41.971	6.768	1461
16(4)	1.6	0	2.30	19.174	3.092	1344
17(4)	1.6	25	2.93	26.778	4.318	1473
18(4)	1.6	50	3.51	33.478	5.399	1538
19(4)	1.6	75	4.16	42.042	6.781	1630
20(4)	1.6	100	4.64	42.997	6.935	1494
21(5)	2.0	0	2.63	23.763	3.833	1457
22(5)	2.0	25	3.20	28.920	4.666	1485
23(5)	2.0	50	3.6	35.829	5.779	1605
24(5)	2.0	75	4.21	42.966	6.926	1645
25(5)	2.0	100	4.65	43.691	7.047	1515

From the data listed in Table 1, the interactive impact of the shell thickness and infill density on the ultimate compressive stress can be graphed, as shown in Fig. 11.

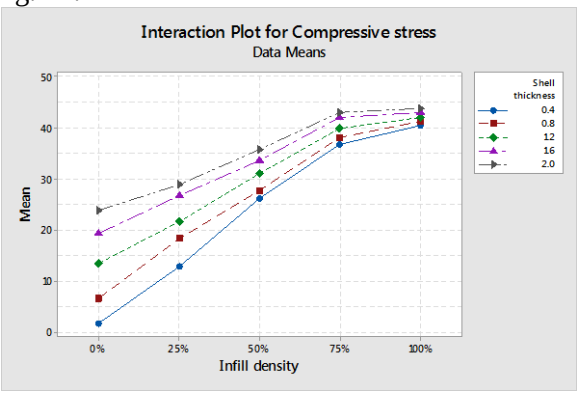

Fig. 11 Interactive impact of shell thickness and infill density on the ultimate compressive strength

As shown in Figure 11, the increase of shell thickness and infill density have an obvious effect on the compressive strength of the samples. Increasing the infill density significantly affects the compressive strength, but this effect decreases to some extent (decreased slope of the curve) after the infill density is 75%, regardless of the shell thickness value. The same behavior was observed for all sample families.

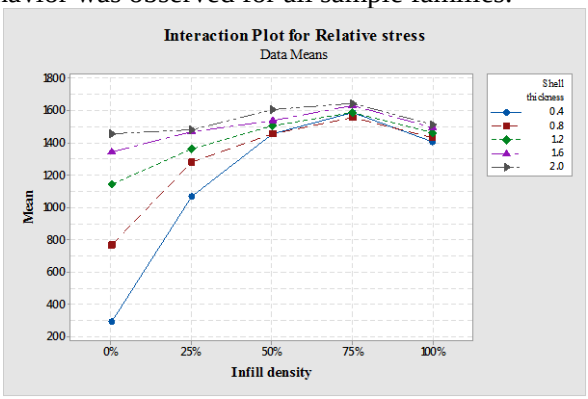

Fig. 12 Interactive impact of shell thickness and infill density on the relative compressive strength

When the relative strength values are considered as shown in Fig. 12, the specimens with an infill density of 75% have the maximum values of relative strength, while increasing the infill density to 100% will decrease the relative strength. This is determined by the increased weight of the specimen with an infill density of 100% compared to similar ones with an infill density of 75% while keeping all other factors constant, which reflects negatively on the value of the relative strength.

The interactive impact of the shell thickness and infill density on the weight of the specimens can be graphed, as shown in Fig. 13.

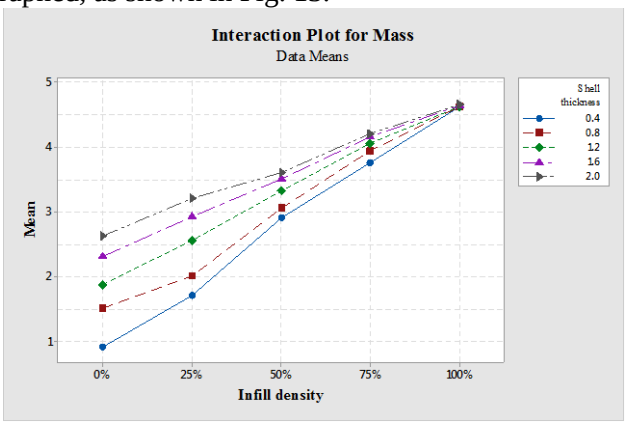

Fig. 13 Interactive impact of shell thickness and infill density on the mass of the specimens

For both infill density and shell thickness, the steep gradient in Fig. 13 shows that the output responses are sensitive to these process parameters. It is noted that the weight of the samples increases with the increase in both the infill density and shell thickness, which is expected behavior as a result of the increase in the raw material.

4.2. Results of the ANOVA Analysis

Minitab calculates a response table for each response characteristic. Response tables can indicate

which factor has the largest impact on the response. Minitab provides three signal-to-noise (S/N) ratios: bigger is better, smaller is better, and nominal is best. Where the appropriate type of ratio is used depends on the type of application. To indicate which factor has the largest influence on the compressive strength (response), (S/N) values (bigger is better) were used as indicated in Equation (2).

$$S/_N = -10\ log\left[\frac{1}{n}\sum_{i=1}^{n}\left(\frac{1}{y_i}\right)^2\right] \quad (2)$$

Table 2 illustrates the response values for the compressive strength.

Table 2 Response for the means of S/N for compressive strength

Level	Shell thickness	Infill density
1	23.53	12.86
2	26.32	21.64
3	29.55	30.83
4	32.89	39.94
5	35.03	42.05
Delta	11.51	29.18
Rank	2	1

According to the statistical analysis of the data in Table 2, the infill density has the greater influence (Rank 1), when compared to the shell thickness (Rank 2). Fig. 14 indicates the S/N of the main effects.

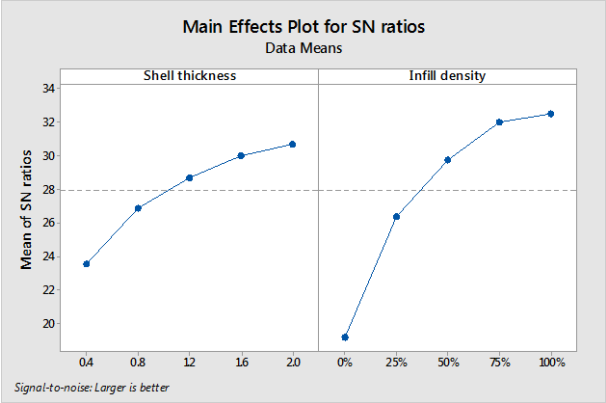

Fig. 14 Main effect plot for S/N ratio on the compressive strength

A visual representation of the main effects of the S/N ratio can be seen in Fig. 14. It is clear that increasing the infill density and shell thickness from low to high levels significantly affects the compressive strength response characteristic values.

S/N values larger is better (Equation 2) were used to indicate which factor has the greatest influence on the relative strength (response). Table 3 shows the response values for S/N ratio for the relative compressive strength.

Table 3 Response for the means of S/N for relative strength

Level	Shell thickness	Infill density
1	1162	1002
2	1301	1335
3	1413	1512
4	1496	1601
5	1541	1462
Delta	380	599
Rank	2	1

According to the statistical analysis of the data in Table 3, the infill density has a greater influence (Rank 1) on relative strength, when compared to the shell thickness (Rank 2). Fig. 15 illustrates the S/N ratios of the main effects.

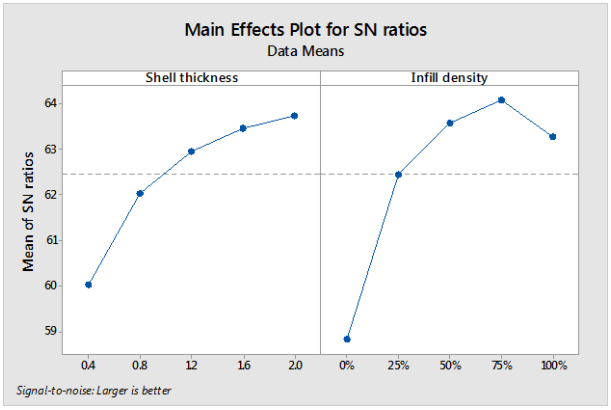

Fig. 15 Main effect plot for S/N ratio on the relative strength

S/N smaller is better; Equation 3 was used to indicate which factor has the greatest influence on the weight of the specimen (response).

$$S/_N = -10\ log\left[\frac{1}{n}\sum_{i=1}^{n}(y)^2\right] \quad (3)$$

Table 4 illustrates the response values for the S/N ratio for the weight of the specimens.

Table 4 Response for the means of S/N for the weight

Level	Shell thickness	Infill density
1	2.776	1.840
2	3.026	2.476
3	3.284	3.278
4	3.508	4.022
5	3.658	4.636
Delta	0.882	2.796
Rank	2	1

According to the statistical analysis of the data in Table 4, the infill density has a greater influence (Rank 1) on the weight of the specimens, while the shell thickness has a lesser one (Rank 2). The S/N ratios of the main effects are shown in Fig. 16.

Figure 16 depicts a visual representation of the main effects of the S/N ratio. It is clear that increasing the infill density and shell thickness from low to high levels significantly affects the weight of the specimens' characteristic values.

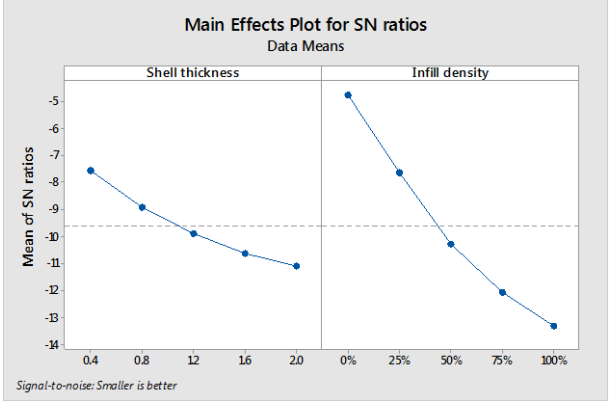

Fig. 16 Main effect plot for S/N ratio on the weight of the specimens

4.3. Predictive Models of Response

For the experimental results listed in Table 1, quadratic mathematical models were formulated to develop a functional relationship between the process control parameters and the response characteristics. Two-factor interaction was used to develop quadratic-fit mathematical models. Equation (4) is a multiple quadratic regression-fitted equation that models the relationship between the response (Y) and the process factors (Xi):

$$Y = -3.98 + 13.494X_1 + 0.6064X_2 - 0.001534X_2^2 - 0.1219X_1 \times X_2 \quad (4)$$

where:
Y - ultimate compressive stress;
X_1 - shell thickness;
X_2 - infill density.

For particular infill density values and shell thickness values, the ultimate compressive stress can be predicted using Equation (4).

A multiple regression-fit Equation (5), models the association between the X factors and Y (relative strength):

$$Y = -0.644 + 2.177X_1 + 0.09788X_2 - 0.000247X_2^2 - 0.01971X_1 \times X_2 \quad (5)$$

where:
Y - relative compressive stress;
X_1 - shell thickness;
X_2 - infill density.

Relative strength can be predicted using Equation (5) for particular infill density and shell thickness values.

The multiple regression-fit Equation (6) models the relationship between Y (weight of the specimen) and the X factors:

$$Y = 0.4093 + 1.2861X_1 + 0.0446X_2 - 0.0848X_1^2 - 0.000031X_2^2 - 0.01092X_1 \times X_2 \quad (6)$$

where:
Y - the weight of the specimen;
X_1 - shell thickness;
X_2 - infill density.

Equation (6) can be used to predict the weight of the specimen for specific values of the infill density and shell thickness factors.

Four additional statistical tests were carried out to compare the measured results with the predicted results to assess the suitability of the fitted regression models for compressive strength, relative strength, and weight of the specimens. The outcomes of these tests are displayed in Table 5.

Table 5 Experimental results versus those predicted

Specimen	Response	Measured	Predicted	Error %
1	Compressive	12.381	11.957	3.4
Infill 20%	Relative	1.984	1.928	2.8
Shell 0.40	Mass	1.78	1.702	4.3
2	Compressive	25.203	24.716	4.8
Infill 40%	Relative	4.192	3.987	4.9
Shell 0.80	Mass	2.88	2.769	3.8
Continuation of Table 5				
3	Compressive	35.636	34.298	3.7
Infill 60%	Relative	5.902	5.533	6.2
Shell 1.2	Mass	3.78	3.609	4.6
4	Compressive	42.268	40.648	3.8
Infill 80%	Relative	6.811	6.566	3.6
Shell 1.6	Mass	4.36	4.222	3.1

Based on Table 5, the two-factor fitted interaction models seem to adequately represent all the considered responses.

5. Conclusions

This work is a step toward enhancing the multipurpose FDM process for ABS prints to obtain good mechanical properties from a sustainability standpoint, by decreasing the number of raw materials used. Through simultaneous analysis and evaluation, the combined effect of shell thickness and infill density on the mechanical properties in the compression of the prints was determined. The strength of 3D-printed specimens was found to be significantly influenced by infill density and shell thickness. The investigational outcomes reveal that the ultimate compressive strength is primarily affected by infill density, whereby it increases with increasing infill density. From the data obtained, it can be concluded that it is not recommended to print the parts with a shell thickness of less than 0.8 mm, as well as that the infill density should not be less than 50%, as the printed parts will have less resistance to stresses and will not withstand loads. It has been determined that further increasing the infill value (from 75% up to 100%) will lead to a slight increase that does not exceed 2% for the compressive stress but will significantly increase the mass of the part by 10.5%. Thus, an infill rate of 75% will be appropriate in terms of durability and lightweight.

Based on the data, it can be concluded that the combination of 2 mm shell thickness with 75% infill density shows substantial relative strength, while 0.4 mm shell thickness with 0% infill density delivers the lowest. The collected data can be used as a reference by FDM 3D printer users when designing and manufacturing 3D printed objects.

The infill density significantly impacts all the considered response variables, namely, compressive strength, relative strength, and material consumption while the shell thickness has a minimal impact. Therefore, it is necessary to invest time and material in the infill density.

The results obtained by comparing the measured data with the predicted data (Table 5) confirm that the quadratic fit model presented in this study is appropriate for determining the relationship between the process factors and the outputs, and it was suitable for all experimental responses.

The results show that the actual values obtained through the experiments are very close to the expected values according to the proposed models with an

insignificant error (a maximum error of 4.8% for compressive strength, 6.2% for relative strength, and 4.6% for weight), as shown in Table 5. The accuracy of the results can be considered as evidence of the validity and adequacy of the developed mathematical models.

6. Limitations and Future Directions

The limitations in this study can be identified using compressive stress as a foundation for the investigation and analyzing the durability of printed parts, and by using two process variables as well as quadratic regression models to predict the responses. While it is possible as a future direction to investigate the effect of other process parameters such as the filling pattern or layer thickness, on other stresses such as tensile stress or bending stress, on the other hand, cubic regression models can be developed to predict the responses.

Acknowledgments

The experiments were carried out at the University of Technology, Department of Production Engineering and Metallurgy, Baghdad, Iraq.

References

[1] TOFAIL S A M, KOUMOULOS E P, BANDYOPADHYAY A, et al. Additive manufacturing: scientific and technological challenges, market uptake and opportunities, *Materials Today*, 2018, 21: 22-37.

[2] JANDYAL A, CHATURVEDI I, WAZIR I, et al. 3D printing – A review of processes, materials, and applications in industry 4.0. *Sustainable Operations and Computers*, 2022, 3: 33-42.

[3] ZHANG, Y, WU, L, GUO, X. et al. Additive Manufacturing of Metallic Materials: A Review. *Journal of Materials Engineering and Performance*, 2018, 27: 1-13.

[4] ROUF S, MALIK A, SINGH N, et al. Additive manufacturing technologies: Industrial and medical applications. *Sustainable Operations and Computers*, 2022, l3: 258-274.

[5] SPAHIU T, ALMEIDA H, MANAVIS A, and KYRATSIS P. Fashion products through digital manufacturing – a case study with FDM technology. *Academic Journal of Manufacturing Engineering*, 2020, 18(4), 63-72.

[6] KRISTIAWAN R B, ARIAWAN F I D, UBAIDILLAH, and ARIFIN Z. A review on the fused deposition modeling (FDM) 3D printing: Filament processing, materials, and printing parameters. *Open Engineering*, 2021, 11: 639-649.

[7] ABBAS T F, ALI H B., & MANSOR K K. Influence of FDM Process Variables on Tensile Strength, Weight, and Actual Printing Time When Using ABS Filament. *International Journal of Modern Manufacturing Technologies*, 2022, 1: 7-13.

[8] ABEYKOON, C, SRI-AMPHORN, P, & FERNANDO, A. Optimization of fused deposition modeling parameters for improved PLA and ABS 3D printed structures. *International Journal of Lightweight Materials and Manufacture*, 2020, 3: 284-297.

[9] VICENTE, CMS, MARTINS, TS, LEITE, M, et al. Influence of fused deposition modeling parameters on the mechanical properties of ABS parts. *Polymers for Advanced Technologies*, 2020, 31: 501-507.

[10] OUDAH S A, AL-ATTRAQCHI H B, & NASSIR N A. The Effect of Process Parameters on the Compression Property of Acrylonitrile Butadiene Styrene Produced by 3D Printer. *Engineering and Technology Journal*, 2022, 40: 189-194.

[11] NGO T D, KASHANI A, IMBALZANO G, et al. Additive manufacturing (3D printing): A review of materials, methods, applications, and challenges. *Composites Part B: Engineering*, 2018, 143: 172-196.

[12] MIKULA, K, SKRZYPCZAK, D, & IZYDORCZYK, G. 3D printing filament as a second life of waste plastics—a review. *Environmental Science and Pollution Research*, 2021, 28: 12321-12333.

[13] YADAV D K, SRIVASTAVA R, & DEV S. Design & fabrication of ABS part by FDM for automobile application. *Materials Today*, 2020, 26: 2089-2093.

[14] ALSOUFI M S, & EL-SAYED A. Warping Deformation of Desktop 3D Printed Parts Manufactured by Open Source Fused Deposition Modeling (FDM) System. *International Journal of Mechanical & Mechatronics Engineering*, 2017, 17: 7-16.

[15] TANVEER Md Q, MISHRA G, MISHRA S, & SHARMA R. Effect of infill pattern and infill density on mechanical behaviour of FDM 3D printed Parts- a current review. *Materials Today: Proceedings*, 2022, 62: 100-108.

[16] STUDDERS C, FRASER I, GILES J W, & WILLERTH S M. Evaluation of 3D-printer settings for producing personal protective equipment. *Journal of 3D Printing in Medicine*, 2021, 5(2): 133-144.

[17] DOBOS J, HANON M M, and OLDAL I. Effect of infill density and pattern on the specific load capacity of FDM 3D-printed PLA multi-layer sandwich. *Journal of Polymer Engineering*, 2022, 42: 118-128.

[18] PANDŽIĆ A, HODŽIĆ D, & KADRIĆ E. Experimental Investigation on Influence of Infill Density on Tensile Mechanical Properties of Different FDM 3D Printed Materials. *TEM Journal*, 2021, 10: 1195-1201.

[19] ABBAS, T.F., MANSOR, K.K., & ALI, H.B. The Effect of FDM Process Parameters on the Compressive Property of ABS Prints. *Journal of Hunan University Natural Sciences*, 2022, 49(7): 154-162.

[20] SHEORAN A J and KUMAR H. Fused Deposition modeling process parameters optimization and effect on mechanical properties and part quality: Review and reflection on present research. *Materials Today: Proceedings*, 2020, (21): 1659-1672.

[21] GAO G, XU F, XU J, and LIU Z. Study of Material Color Influences on Mechanical Characteristics of Fused Deposition Modeling Parts. *Materials (Basel)*, 2022, 15(19): 7039.

参考文:

[1] TOFAIL S A M 、 KOUMOULOS E P 、 BANDYOPADHYAY A 等。增材制造：科技挑战、市场吸收和机遇，今日材料，2018，21：22-37。

[2] JANDYAL A、CHATURVEDI I、WAZIR I 等。3 丁打印——工业 4.0 中的流程、材料和应用回顾。可持续运营与计算机，2022，3：33-42。

[3] ZHANG, Y, WU, L, GUO, X. 等。金属材料的增材制造：综述。材料工程与性能学报, 2018, 27: 1-13.

[4] ROUF S、MALIK A、SINGH N, 等人。增材制造技术：工业和医疗应用。可持续运营和计算机，2022，l3：258-274。
[5] SPAHIU T 、 ALMEIDA H 、 MANAVIS A 和 KYRATSIS P. 通过数字化制造的时尚产品——频分复用技术案例研究。制造工程学术期刊, 2020, 18(4), 63-72.
[6] KRISTIAWAN R B 、 ARIAWAN F I D 、 UBAIDILLAH 和 ARIFIN Z。关于熔融沉积建模(频分复用) 3 丁打印的评论：灯丝加工、材料和打印参数。开放工程，2021，11：639-649。
[7] ABBAS T F、ALI H B.、和 MANSOR K K. 使用防抱死制动系统长丝时频分复用工艺变量对拉伸强度、重量和实际打印时间的影响。国际现代制造技术杂志, 2022, 1: 7-13.
[8] ABEYKOON, C, SRI-AMPHORN, P, 和 FERNANDO, A. 优化熔融沉积建模参数以改进解放军和防抱死制动系统 3 丁打印结构。国际轻质材料与制造杂志，2020，3：284-297。
[9] VICENTE C M S, MARTINS T S, LEITE M 等。熔融沉积建模参数对防抱死制动系统部件机械性能的影响。用于先进技术的聚合物，2020，31：501-507。
[10] OUDAH S A, AL-ATTRAQCHI H B, 和 NASSIR N A. 工艺参数对 3 丁打印机生产的丙烯腈丁二烯苯乙烯压缩性能的影响。工程技术杂志, 2022, 40: 189-194.
[11] NGO T D, KASHANI A, IMBALZANO G, 等。增材制造（3 丁打印）：对材料、方法、应用和挑战的回顾。复合材料乙部分：工程，2018，143：172-196。
[12] MIKULA, K, SKRZYPCZAK, D, 和 IZYDORCZYK, G. 3 丁打印长丝作为废塑料的第二次生命——综述。环境科学与污染研究, 2021, 28: 12321-12333.
[13] YADAV D K, SRIVASTAVA R, 和 DEV S. 通过频分复用为汽车应用设计和制造防抱死制动系统零件。今日材料，2020，26：2089-2093。
[14] ALSOUFI M S, 和 EL-SAYED A. 由开源熔融沉积建模(频分复用)系统制造的桌面 3 丁打印部件的翘曲变形。国际机械与机电工程杂志, 2017, 17: 7-16.
[15] TANVEER Md Q、MISHRA G、MISHRA S 和 SHARMA R. 填充图案和填充密度对频分复用 3 丁打印部件机械行为的影响 - 当前评论。今日材料：会议记录，2022，62：100-108。
[16] STUDDERS C 、 FRASER I 、 GILES J W 和 WILLERTH S M。评估用于生产个人防护设备的 3 丁打印机设置。医学 3 丁打印杂志，2021，5(2)：133-144。
[17] DOBOS J、HANON M M 和 OLDAL I. 填充密度和图案对频分复用 3 丁打印解放军多层三明治的比负载能力的影响。高分子工程学报, 2022, 42: 118-128.
[18] PANDŽIĆ A、HODŽIĆ D 和 KADRIĆ E. 填充密度对不同频分复用 3 丁打印材料拉伸机械性能影响的实验研究。透射电镜期刊，2021，10：1195-1201。
[19] ABBAS, T.F.、MANSOR, K.K. 和 ALI, H.B. 频分复用工艺参数对防抱死制动系统打印件压缩性能的影响。湖南大学自然科学学报, 2022, 49(7): 154-162.
[20] SHEORAN A J 和 KUMAR H. 熔融沉积建模工艺参数优化及其对机械性能和零件质量的影响：对当前研究的回顾和反思。今日材料：会议记录，2020， (21)：1659-1672。
[21] GAO G、XU F、XU J 和 LIU Z. 材料颜色对熔融沉积成型零件机械特性影响的研究。材料（巴塞尔），2022，15（19）：7039。